Role of magnetism in Cu precipitation in α-Fe

O. I. Gorbatov,[1,2,3,4] I. K. Razumov,[1,4] Yu. N. Gornostyrev,[1,4] V. I. Razumovskiy,[2,5] P. A. Korzhavyi,[2] and A. V. Ruban[2]

[1]*Institute of Quantum Materials Science, Ekaterinburg 620107, Russia*

[2]*Department of Materials Science and Engineering, KTH Royal Institute of Technology, SE-100 44 Stockholm, Sweden*

[3]*Magnitogorsk State Technical University, Magnitogorsk 455000, Russia*

[4]*Institute of Metal Physics, Ural Division RAS, Ekaterinburg 620219, Russia*

[5]*Materials Center Leoben Forschung GmbH, Roseggerstraße 12, A-8700 Leoben, Austria*

(Received 25 June 2013; revised manuscript received 14 October 2013; published 25 November 2013)

The temperature-dependent solubility of Cu in α-Fe and initial stages of Cu precipitation are investigated in first-principles calculations and statistical thermodynamic and kinetic modeling based on *ab initio* effective interactions. We demonstrate that the weakening of the phase separation tendency with increasing temperature, especially close to the magnetic phase transition, is related to the strong dependence of the "chemical" interactions on the global magnetic state. At the same time, our calculations demonstrate that the vibrational contribution obtained in the quasiharmonic approximation is relatively small for temperatures near the Curie point. The results of Monte Carlo simulations of Cu solubility and clustering are in good agreement with experimental data.

DOI: 10.1103/PhysRevB.88.174113 PACS number(s): 64.70.kd, 64.75.Nx, 75.50.Bb

I. INTRODUCTION

Alloying is one of the major approaches to improving the properties of low-carbon steels[1] for modern pipelines or naval applications. Copper has long been used as an alloying element for improving the corrosion resistance of steel. However, an excess of copper can result in extra hardening and embrittlement due to copper precipitation, which is greatly accelerated under irradiation in reactor pressure vessel steels.[2–4] During the last decade, the interest to copper alloying has been reinforced since a new steel grade was designed[5] in which high values of ductility and fracture toughness were attained using precipitation strengthening by nanometer-sized copper-rich particles formed in the α-Fe matrix during cooling. Although the strengthening effect of copper precipitates has been known for a long time,[6] the mechanism of this phenomenon, as well as the factors controlling the formation of nanometer-sized copper-reach inclusions, are still under debate (see, e.g., Refs. 7 and 8).

The kinetics of decomposition of supersaturated Fe-Cu-based alloys has been a subject of numerous experimental studies where Cu-rich precipitates were formed either during annealing[9–22] or under irradiation.[23–43] It has been established that precipitation occurs in several stages.[9,10,44–46] An early stage typically involves the formation of nanometer-sized coherent Cu-rich precipitates, which adopt the bcc structure of the alloy. Next, upon growing in size, the precipitates are observed to transform into a close-packed phase with the 9*R* crystal structure[47] ($C19$ or α-Sm structure type: a twinned lattice with a nine-layer-repeated stacking sequence) and, finally, to the fcc structure upon further increasing the annealing/exposure time.

Despite intensive research during the last decade,[14–17,20,21,48–50] the composition of nanosized precipitates in Fe-Cu alloys is still under debate (see discussion in Ref. 8). According to several 3D atom-probe tomographic studies,[15,29,30,49,50] the nanometer-sized precipitates with bcc lattice contain about 50 at.% of Cu (for a more thorough discussion of this method see Refs. 17,49 and 50). At the same time, positron annihilation[51] and neutron scattering studies[8] have indicated that precipitates might contain much less Fe. As is commonly accepted now, the nanometer-sized precipitates appear strongly undersaturated with Cu in atom probe measurements. However, the reason of this phenomenon remains unclear.

The pronounced effect of bcc-Cu precipitates on the mechanical properties of α-Fe has stimulated researchers to study the thermodynamic properties and precipitation of Fe-Cu solid solutions. Several approaches were employed for studying the kinetics of decomposition in the Fe-Cu system at different time and length scales. The phase-field method (PFM) was used in Refs. 52–55 for simulating microstructural evolution, including precipitate growth, in Fe-Cu alloys. However, PFM uses a large number of phenomenological parameters, which are often uncertain.[56] More reliable results were obtained in the framework of stochastic statistical theory,[57,58] which uses the effective interactions (EI) chosen by fitting to the experimental data such as the cohesive and mixing energies. Besides, Monte Carlo (MC) modeling studies with simplified interactions[59–68] yield a qualitatively accurate description of precipitation kinetics, although they have not yet provided a physically sound explanation of the experimental results on precipitate composition.[15,29,30,49,50]

Theoretical modeling approaches based on first-principles calculations and atomistic simulations are now becoming valuable research tools in the investigations of structure, energetics, and physical properties of alloys. With the aim of deriving a first-principles parametrization of the total energy in terms of a cluster expansion, the authors of Ref. 69 performed a systematic study of various atomic configurations in bcc Fe-Cu alloys using calculations based on density functional theory (DFT). A satisfactory agreement was found between the calculated and experimental mixing enthalpies. An instability of the bcc crystal lattice was noticed for the copper-rich Fe-Cu solid solutions with $c_{Cu} > 50\%$, for which the elastic modulus C' was calculated to be negative. This finding is important for understanding the evolution of copper precipitates in iron. However, the calculations of Ref. 69 were performed for rather concentrated alloys, $c_{Cu} > 20\%$, while the description of early stages of the decomposition requires the knowledge of interaction parameters in dilute Fe-Cu solid solutions.

The energies of pairwise interactions between Cu atoms in the ferromagnetic matrix of bcc Fe have been determined *ab initio*, using the density functional theory calculations.[63,64,70,71] It was found that the Cu-Cu interactions are attractive, strong, and short-ranged. However, these interactions significantly underestimated the solubility of Cu in bcc Fe,[64] and the obtained mismatch between theory and experiment at high temperatures in the paramagnetic (PM) state was ascribed to an unaccounted entropy contribution. As shown in Refs. 72–74, the disagreement between theory and experiment at high temperatures can be reduced by taking into account a vibrational free energy contribution.

Nevertheless, this interpretation cannot be regarded as a solution of the problem since the theoretical model proposed in these papers[72–74] disregards the effect of magnetic disorder, treating the Fe-Cu system above the Curie temperature in the low-temperature ferromagnetic (FM) state. In fact, there is clear evidence of the impact of magnetic order-disorder transition upon the Cu solubility in α-Fe: the solubility exhibits a strongly non-Arrhenius behavior near the Curie temperature.[75–78] This behavior can hardly be explained solely by the vibrational contribution evaluated for a *frozen* magnetic state. The observed variation of the apparent solution energy of Cu in Fe also implies that the EI in the system should depend on the magnetic state[79] (or degree of magnetic order) and change with temperature near the Curie point, T_C, as is established in first-principles calculations for Fe-Cr[80,81] and other iron-based alloys.[82–85]

In fact, the effect of magnetism on thermodynamic properties of alloys has been a subject of special attention since the classical papers by C. Zener[86,87] whose ideas have been further developed on a phenomenological level in Refs. 75,78, and 88–95. Thus a consistent *ab initio* description of Fe-Cu solid solutions requires a careful analysis of all the relevant degrees of freedom, and especially the magnetic one, whose energy is of the same order as the chemical energy change due to a phase transformation.[96]

In order to elucidate the effect of magnetism on the decomposition of Fe-Cu alloys, we employ a combined modeling approach, which involves first-principles calculations of the energetics of Fe-Cu alloys, including the vibrational and magnetic contributions to the EI, and subsequent statistical-mechanical (Monte Carlo) simulations of Cu precipitation. We show that the EI in Fe-Cu alloys vary nonlinearly with temperature, following the behavior of magnetization, and namely the temperature dependence of the chemical interactions produces the main effect on the solubility of Cu at high temperatures.

The remainder of this paper is organized as follows. In Sec. II, we give details of the calculations. The calculated mixing and solution energies (including the effect of lattice vibrations in the quasiharmonic approximation) are presented in Sec. III, where a justification is provided for neglecting the vibrational contribution in our subsequent calculations. The obtained solution energies are used for evaluating the Cu solubility limit in the mean-field approximation. In Sec. IV, effective interactions are calculated, and their dependence on temperature and composition is discussed. The interactions obtained in Sec. IV are used in Monte Carlo simulations of the solid solution decomposition presented in Sec. V. In the same section, the simulation results are compared with the available experimental and theoretical data, and the role of magnetism in the thermodynamics and the kinetics of precipitation is discussed.

II. METHODOLOGY

A. First-principles techniques

1. Exact muffin-tin orbital method calculations

The exact muffin-tin orbitals (EMTO) method[97–100] has been used to calculate electronic structure, total energies and EI in random bcc Fe-Cu alloys. Substitutional disorder in the alloys has been treated within the coherent potential approximation (CPA).[101] The accuracy of the CPA has been checked in the corresponding locally self-consistent Green's function (LSGF) calculations[102,103] and EMTO-LSGF.[104] The LSGF method has also been used to determine the parameters (screening constants) describing the contributions of screened Coulomb interactions to the one-electron potential $V_i^{\rm scr}$ of alloy component i and to the total energy $E_{\rm scr}$ within the single-site DFT formalism:[105]

$$V_i^{\rm scr} = -\alpha_{\rm scr}\frac{e^2 q_i}{S} \quad \text{and} \quad E_{\rm scr} = \frac{\beta_{\rm scr}}{2}\sum_i c_i q_i V_i^{\rm scr}. \tag{1}$$

Here, e is the electron charge, S is the Wigner-Seitz radius, and q_i and c_i are the average net charge of the atomic sphere and the concentration for the ith alloy component, respectively. The calculated screening constants are $\alpha_{\rm scr} = 0.92$ and $\beta_{\rm scr} = 1.15$ in the FM state and $\alpha_{\rm scr} = 0.86$ and $\beta_{\rm scr} = 1.15$ in the PM state.

The PM state is described by a disordered local moment (DLM) model[106,107] in which each alloy component is represented by its spin-up ($\uparrow$) and spin-down ($\downarrow$) species that are assumed to be distributed randomly on the underlying lattice. The FM state with reduced magnetization, m, have been described by a partially disordered local moment (PDLM) model[80] in which a binary $Fe_{1-c}Cu_c$ is presented by a random ternary alloy $(Fe_x^{\uparrow}\, Fe_{1-x}^{\downarrow})_{1-c}Cu_c$, where

$$x = \frac{1+m}{2}. \tag{2}$$

The total energies were determined in the generalized gradient approximation[108] (GGA) using the full charge density (FCD) formalism.[100] All the self-consistent EMTO-CPA calculations were performed by using an orbital momentum cutoff of $l_{\rm max} = 3$ for partial waves. The integration over the Brillouin zone was done using $25 \times 25 \times 25$ grid of $\mathbf{k}$ points determined according to the Monkhorst-Pack scheme.[109] The convergence of the results was checked by increasing the $\mathbf{k}$-point grid up to $41 \times 41 \times 41$ in some calculations.

The energies of alloy are defined by the following configurational Hamiltonian:

$$\begin{aligned} H_{\rm conf} = {} & \frac{1}{2}\sum_p V_p^{(2)} \sum_{i,j\subset p} \delta c_i \delta c_j \\ & + \frac{1}{3}\sum_t V_t^{(3)} \sum_{i,j,k\subset t} \delta c_i \delta c_j \delta c_k \\ & + \frac{1}{4}\sum_q V_q^{(4)} \sum_{i,j,k,l\subset q} \delta c_i \delta c_j \delta c_k \delta c_l, \end{aligned} \tag{3}$$

where $V_p^{(2)}$, $V_t^{(3)}$, and $V_q^{(4)}$ are the two-, three- and four-site interactions for the corresponding two-, three-, and four-site clusters denoted by p, t, and q. The δc_i are the concentration fluctuations at sites i; $\delta c_i = p_i - c$, where p_i is the occupation number at site i, taking on values 1 or 0 if the site i is occupied by an Fe or Cu atom, respectively.

The chemical contribution to the EI on a fixed ideal underlying lattice has been determined by the screened generalized perturbation method (SGPM)[105,110] using the EMTO-CPA self-consistent one-electron potentials of alloy components. In the case of EI, it consists of two contributions: one from the one-electron energies $V^{(2)}_{\text{one-el}}(\mathbf{R})$ (see Refs. 105 and 110) and the other from screened Coulomb interactions $V_{\text{scr}}(\mathbf{R})$:

$$V_n^{(2)-\text{ch}} \equiv V^{(2)-\text{ch}}(\mathbf{R}_n) = V^{(2)}_{\text{one-el}}(\mathbf{R}_n) + V^{\text{scr}}(\mathbf{R}_n), \quad (4)$$

where n is the coordination shell, which corresponds to sites $\mathbf{R}_n$, and

$$V^{\text{scr}}(\mathbf{R}) = e^2\alpha^{\text{scr}}(\mathbf{R})\frac{q_{\text{eff}}^2}{S}. \quad (5)$$

Here, $q_{\text{eff}} = q_{\text{Cu}} - q_{\text{Fe}}$ is the effective charge transfer between Cu and Fe and $\alpha^{\text{scr}}(\mathbf{R} \neq 0)$ are the intersite screening constants, which have been determined in the corresponding LSGF supercell calculations for different alloy compositions and magnetic states. In particular, the values of $\alpha^{\text{scr}}(\mathbf{R}_n)$ for the first three coordination shells in the dilute limit of FM (DLM) Fe-rich Fe-Cu random alloy are found to be 0.1090 (0.1131), 0.0143 (0.0252), 0.0028 (−0.0028). The intersite screening constants for concentrated alloys ($6.25 < c < 50$ at.% Cu) have been determined from a fit to the calculated ordering energies of some ordered structures (e.g., $B2$, $B32$, and $D0_3$). The screening constants determined in this way were 0.0226, 0.0050, and −0.0006 for the first three coordination shells, respectively, both in the FM and DLM states. In some cases, especially when considering high temperatures, we have used experimental lattice parameters[111–114] in the first-principles calculations of EI and solution energies.

2. *Projector augmented wave method calculations*

The full-potential projector augmented wave (PAW) method[115,116] as implemented in the Vienna *ab initio* simulation package (VASP)[117–120] has been used in several calculations, namely, to compute the Cu solution energy at 0 K, to calculate the force constants of Fe, Cu, and Fe-Cu alloys for subsequent lattice dynamics calculations (to model the vibrational contribution to the solution energy at finite temperatures), as well as to evaluate the strain-induced and vibrational contributions to the effective pair interactions.

In particular, the strain-induced interactions V_n^{si} have been obtained as the difference of the relaxation energies around a pair of Cu atoms separated by the distance of nth coordination shell, $\Delta E_{\text{rel}}^{\text{Cu-Cu}}(\mathbf{R}_n)$, and that for a single Cu impurity atom, $\Delta E_{\text{rel}}^{\text{Cu}}$, in a supercell of otherwise pure Fe (see Refs. 121 and 122):

$$V_n^{\text{si}} = \Delta E_{\text{rel}}^{\text{Cu-Cu}}(\mathbf{R}_n) - 2\Delta E_{\text{rel}}^{\text{Cu}}. \quad (6)$$

For that purpose, we have used a 128-atom $4 \times 4 \times 4$ supercell built upon a cubic bcc unit cell consisting of two atoms. The total energy calculations have been done in the GGA with the kinetic energy cutoff of 350 eV and using a uniform $4 \times 4 \times 4$ Monkhorst-Pack mesh of $\mathbf{k}$ points. The calculations of the strain-induced interactions have been done in the FM state, thereby assuming that the strain-induced interactions in the PM state are the same. We believe it is a reasonable approximation, because strain-induced interactions are mostly due to the size mismatch of the alloy components which is only slightly affected by the magnetic state. This approach has been previously applied to iron-based systems.[123,124]

The PAW method has also been used in the total energy calculations of random $Fe_{0.875}Cu_{0.125}$, $Fe_{0.75}Cu_{0.25}$, and $Fe_{0.50}Cu_{0.50}$ alloys. They have been modeled by supercells of different sizes. In particular, a 128-atom supercell formed by $4 \times 4 \times 4$ translations of a two-atom ($\times 2$) cubic unit cell of the bcc structure was used in calculations of $Fe_{0.875}Cu_{0.125}$ and $Fe_{0.75}Cu_{0.25}$, while a 64-atom supercell ($4 \times 4 \times 4$) built upon a bcc primitive unit cell was used to model the $Fe_{0.50}Cu_{0.50}$ random alloy.

In order to keep the cubic symmetry of the underlying bcc lattice, which is preserved on average in real alloys, the shape of the unit cells was kept fixed while all the atomic positions inside the supercell were relaxed until the forces acting on atoms were less than 10^{-2} eV/Å. The GGA[108] has been used in the PAW self-consistent calculations. The convergence criterion for the total energy was 10^{-5} eV. To avoid systematic errors, the total energies of pure elements in the PAW calculations of the mixing energies of a particular alloy have been calculated using the same supercells and parameters of the PAW method as in the total energy calculations for the corresponding alloy.

B. Monte Carlo simulations

In the present work, we perform two different types of Monte Carlo (MC) simulations of decomposition in the Fe-Cu alloys. To simulate alloy thermodynamics, we have used the Monte Carlo[125] method in the canonical ensemble exchanging randomly chosen Fe and Cu atoms. This algorithm provides a quick way to achieve the equilibrium distribution of atoms in simulations.

The simulation box in Monte Carlo calculations was $80 \times 80 \times 80$ built upon on the primitive bcc unit cell. For each alloy composition, the simulation began from a random distribution generated at high temperature, and then the temperature was lowered down in small steps. At each temperature, the system was first equilibrated for 3000 MC steps/atom. After that, the mean values of the total energy, heat capacity, and correlation functions were obtained by averaging over additional 6000 MC steps/atom.

In order to simulate the kinetics of Cu precipitation, we have used a simplified but fast lattice kinetic Monte Carlo method based on Kawasaki dynamics.[126] Within this scheme, a pair of Cu and Fe atoms are exchanged in accordance with the MC algorithm only if they are nearest neighbors. Let us note that the use of a more general kinetic Monte Carlo (KMC) approach,[127] which employs realistic vacancy-mediated exchange of alloy components, is quite time consuming in the case of dilute alloys as it may require a huge number of atomic-vacancy exchanges to change the alloy configuration.

In Kawasaki dynamics, the time of the decomposition process is expressed in terms of the number of elementary atom rearrangements. The real time scale can be established from a relation between the impurity diffusion coefficient D_i of the solute atom in the matrix and the time τ needed for a successful jump of a Cu atom into the nearest-neighbor position:

$$D_i = \frac{d^2}{\tau}. \tag{7}$$

To determine the time constant τ, we have used the nearest-neighbor distance in bcc Fe $d = 1.46$ Å and experimental data on the temperature dependence of the impurity diffusion coefficient D_i for Cu in Fe, as represented by Jönsson's model.[93,94] The model takes accurately into account the non-Arrhenius behavior of the self-diffusion and impurity diffusion coefficients near the critical temperature of magnetic ordering in iron. For temperatures below T_C the model yields values of the Cu impurity diffusion coefficient that are rather close to the values calculated in Ref. 64, but some two orders of magnitude lower than those used in Ref. 128.

III. MIXING AND SOLUTION ENERGIES

A. Magnetic and chemical contributions

Since Fe-Cu alloys do not form ordered interemetallic compounds, the main thermodynamic quantity characterizing the solubility of the solute (Cu), as well as the stability of the solid solution with respect to decomposition, is the enthalpy of formation (or the mixing energy) of the random alloy at zero pressure $P = 0$. The mixing energy is defined as the difference between the total energy of a random alloy $E_{\mathrm{Fe}_{1-c}\mathrm{Cu}_c}$ and the weighted sum of total energies of the pure components, E_{Fe} and E_{Cu}, calculated in the same bcc structure:

$$E_{\mathrm{mix}}(c) = E_{\mathrm{Fe}_{1-c}\mathrm{Cu}_c} - (1-c)E_{\mathrm{Fe}} - cE_{\mathrm{Cu}}. \tag{8}$$

In the upper panel of Fig. 1, we show the mixing energy of Fe-Cu alloys calculated in the DLM and FM states by the EMTO method in the GGA. The results for the FM state are in good agreement with PAW method calculations using 128-atom supercells (the results are shown in the Figure) as well with PAW results reported previously.[69] Although the mixing energies calculated in the DLM and FM states seem to be close to each other, their detailed concentration dependencies in the dilute limit of Cu are quite different. This is better seen in the lower panel of Fig. 1 where we plot another quantity, the effective mixing potential $W_{\mathrm{mix}}(c) = E_{\mathrm{mix}}(c)/[c(1-c)]$. Although W_{mix} is almost constant in the DLM state for the whole composition range, in the FM state, it changes abruptly close to pure Fe.

Such an abrupt change of the mixing potential is a clear indication of a strong concentration dependence of the EI. Indeed, in the absence of the concentration dependence of the effective pair interactions, W_{mix} would a constant that could be expressed (in mean field approximation) as $W_{\mathrm{mix}} = 1/2 \sum_p z_p V_p$, where z_p is the coordination number and V_p the effective pair interaction at the pth coordination shell.

In the dilute limit, the mixing potential $W_{\mathrm{mix}}(c \to 0)$ becomes equal to the impurity solution energy of Cu in Fe (apart from a small addition term, the structural energy difference of the bcc and fcc Cu, which is about 2.6 mRy according to PAW calculations). One can clearly see from the results presented in the lower panel of Fig. 1 that the magnetic state hugely affects the solution energy of Cu impurity in bcc Fe, something which is not visible if one just compares the mixing energies. Our 128-atom supercell PAW-VASP calculations, without relaxing the atomic positions, yield 47.9 mRy for the Cu solution energy at the room temperature lattice constant, the relaxation energy being −1.7 mRy. Our EMTO-LSGF calculations yield 48.2 mRy without local lattice relaxations, which is in good agreement with our PAW results and EMTO-CPA results (see Fig. 1). They are in reasonable agreement with other first-principles results, which are scattered in the range of 32.3–58.1 mRy.[64,70–72,129] Such a large scatter is probably due to sensitivity of the results to the size of the supercell and other details of the calculations.

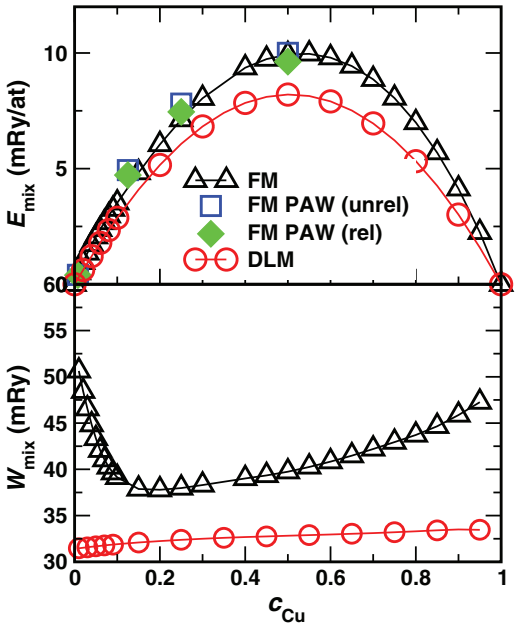

FIG. 1. (Color online) Mixing energy of bcc Fe-Cu random alloys E_{mix} (top) and mixing potential $W_{\mathrm{mix}} = E_{\mathrm{mix}}/[c(1-c)]$ as a function of Cu concentration in the FM and DLM states (bottom). The EMTO-CPA results are shown by circles and triangles, while supercell PAW results by open squares (unrelaxed) and filled diamonds (relaxed).

Let us note that the solution energy in the DLM or paramagnetic state strongly depends on the lattice constant. Being determined at an experimental high-temperature lattice constant, it is about 28.8 mRy at $T = 1000$ K, which is substantially lower than the value of about 33 mRy at the theoretical lattice constant corresponding to $T = 0$ K. We note again that the solution energies calculated in the DLM state do not contain the contribution from lattice vibrations, which is quite difficult to determine.

Independently of the magnetic state, impurities of Cu in the α-Fe matrix exhibit strong tendency towards clustering. The tendency becomes substantially weaker with increasing temperature, which is the result of both, thermal lattice expansion and changing the global magnetic state. Such a dependence should cause a peculiar behavior of the basic

thermodynamic and kinetic alloy properties. This also means that theoretical simulations require the use of the temperature-dependent EI (through magnetization).

B. Effect of lattice vibrations: Quasiharmonic approximation

In this section, we investigate the vibrational contribution to the solution energy $\Delta F_{\rm sol}^{\rm vib}$, which, according to Refs. 72 and 73, is responsible for a substantial increase of the solubility at high temperatures, close to the magnetic phase transition. In doing so, we calculate the phonon free energy of pure bcc Fe, fcc Cu, and dilute bcc Fe-Cu alloys. In order to minimize the systematic computational error, all the calculations are done for 64-atom supercells based on the primitive cell of either bcc structure (cases of pure Fe and Fe-Cu alloys) or fcc structure (the case of pure Cu).

The corresponding force constants have been calculated using the density functional perturbation theory (DFPT)[130–132] as implemented in VASP.[116] The electronic structure self-consistent calculations have been done using a uniform $6\times6\times6$ Monkhorst-Pack mesh of **k** points. The kinetic energy cutoff was 350 eV. The calculations of vibrational properties have been carried out using PHONOPY code.[133,134] The phonon density of states and the vibrational free energies $\Delta F^{\rm vib}$ have been evaluated using a $6\times6\times6$ **q**-point mesh of Monkhorst and Pack.

It is clear that the vibrational contribution is temperature dependent: it is negligible at 0 K, but can be substantial at high temperatures. The simplest way to account for the vibrational contribution is to use a harmonic approximation when the phonon free energy is determined for a fixed lattice constant and a given magnetic state. More accurate consideration can be done using a quasiharmonic approximation, where the vibrational free energy is determined as a function of temperature at several different lattice constants.

In general, one also needs to follow the change of the magnetic state with temperature, which, in particular, has been shown to affect the elastic[135] and vibrational properties of bcc Fe.[136,137] Unfortunately, lattice dynamics calculations for alloys in the PM state are too cumbersome at the present time. Therefore we restrict ourselves here to quasiharmonic treatment of lattice vibrations in the FM state. In order to further simplify our consideration, we use experimental data for the lattice constants of α-Fe and Cu at different temperatures.[113,114] This procedure is accurate enough to obtain a qualitative picture of the thermal expansion effect.

The results are presented in Fig. 2, where we show the contribution from lattice vibrations to the solution energy, calculated as a function of temperature for a set of lattice constants. As one can see, our results for the room temperature lattice parameter of Fe are in good agreement with those obtained by Reith *et al.*[72] at the theoretical 0 K lattice parameter of bcc Fe. That is, if the lattice constant is fixed to the ground-state value, one indeed gets quite substantial *negative* contribution from the lattice vibrations to the solution energy of Cu in Fe near and above the Curie temperature.

At the same time, if one takes into consideration the thermal lattice expansion, the result for the vibrational contribution to the solution energy changes dramatically. It is shown by thick solid line in Fig. 2. As one can see, instead of a linear

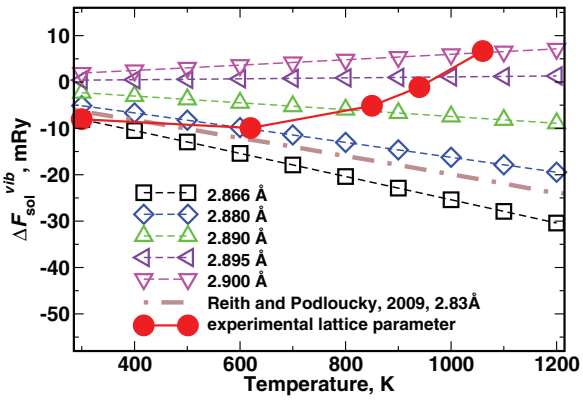

FIG. 2. (Color online) Temperature dependence of the vibrational solution free energy for a single Cu impurity in a 64-atom Fe supercell. The bold solid line is the resulting $F_{\rm sol}^{\rm vib}$ corresponding to experimental temperature-dependent equilibrium lattice parameter. The dash-dotted line shows the result reported by Reith and Podloucky of Ref. 72.

decrease of the vibrational contribution to the solution energy with temperature, one observes its quite substantial nonlinear growth, so that at temperatures close to the magnetic transition it actually becomes *small positive*. It is also clear that the final conclusion about the contribution of lattice vibrations to the solution energy can be drawn only when the corresponding thermal magnetic excitations are properly taken into account in the phonon calculations.

We have also estimated the vibrational contribution to the nearest-neighbor effective pair interaction, which has been obtained in the vibrational free energy calculations of a pair of Cu atoms in two different configurations in the 64-atom supercell. First, the two Cu atoms were placed next to each other, and then they were considered far away from each other (at the most distant coordination shell for the given supercell).

Assuming that vibrational contribution to the effective pair interaction is small at the distant coordination shell, the vibrational contribution to the EI at the first coordination shell is given by the difference of the vibrational total energies. The so-defined vibrational contribution to the solute-solute interaction energy is less than 1 mRy at the lattice parameters corresponding to temperatures in the range 950–1050 K, which is significantly smaller than the effective chemical interactions presented in Sec. IV, and therefore it was neglected in the subsequent calculations.

IV. EFFECTIVE INTERACTIONS

As has been mentioned above, apart from "chemical" interactions that are defined on a rigid undistorted lattice, there can be another contribution, coming from configurationally dependent local lattice relaxations. The contribution is also referred to as the strain-induced interaction. Since the size mismatch between Fe and Cu atoms is small, the strain-induced interactions are also expected to be small. Indeed, the strain-induced interactions $V_n^{\rm si}$, obtained for the first five coordination shells of the bcc lattice in the dilute limit of Cu in Fe, are −0.96, −0.70, 0.03, 0.07, and 0.50 mRy, respectively. In general, they also depend on the volume,

concentration, and temperature. Nevertheless, we assume that such dependencies are negligible, and just add the strain-induced contribution to the chemical interactions obtained from the SGPM calculations.

A. Magnetization dependence of the effective interactions

In the description of magnetic excitations in Fe, we assume that they are mostly transverse magnetic excitations, that are magnons or spin waves at low temperature. At high temperatures, the magnon picture breaks down due to magnon-magnon interactions, and magnetic excitations of another type appear, namely, longitudinal spin fluctuations. However, in bcc Fe, the effect of the latter is relatively little pronounced, so one can still use the Heisenberg approach, but with renormalized magnetic interactions which will now be dependent on the global magnetic state.

The interactions should also depend on the relative orientation of the magnetic moments at two particular sites, as well as on the global magnetization. However, using the PDLM model, one can reduce such a dependence only to two orientations of the local magnetic moment: spin up, which we assume to be aligned with the direction of the global magnetization (i.e., majority spin orientation), and spin down with the opposite orientation. That is, in a partially ordered magnetic state of Fe, there are three different magnetic exchange interactions: $J_p^{\mathrm{Fe}^\uparrow\mathrm{Fe}^\uparrow}$, $J_p^{\mathrm{Fe}^\uparrow\mathrm{Fe}^\downarrow}$, and $J_p^{\mathrm{Fe}^\downarrow\mathrm{Fe}^\downarrow}$, which become equal to each other *only* in the completely random DLM state, where the magnetic Hamiltonian is

$$H_{\mathrm{magn}} = -\sum_p \sum_{i,j\in p} J_p \mathbf{e}_i \mathbf{e}_j. \tag{9}$$

Here, J_p are the magnetic exchange interaction parameters for the pth coordination shell, $\mathbf{e}_i$ the direction of magnetic moments on site i.[138]

In Fig. 3, we show the magnetic exchange interactions, $J_p^{\mathrm{Fe}^\uparrow\mathrm{Fe}^\uparrow}$ and $J_p^{\mathrm{Fe}^\uparrow\mathrm{Fe}^\downarrow}$, for different values of magnetization. As one can see, the magnetic exchange interactions exhibits quite strong dependence on magnetization close to the perfectly ordered FM state ($m = 1$). Such a strong dependence is a clear indication that bcc Fe is not an ideal Heisenberg system in which the magnetic interaction parameters are supposed to be just constants. However, in a more general consideration, if one allows for a magnetization dependence of the magnetic exchange interactions, the Heisenberg picture is still qualitatively reasonable. The dependence of the magnetic exchange interactions in bcc Fe on the magnetic state has been discussed earlier.[110,139]

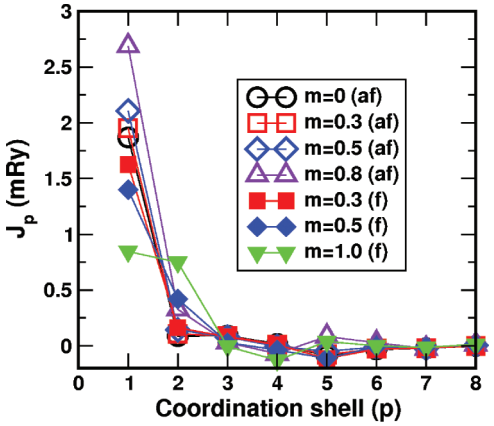

FIG. 3. (Color online) Magnetic exchange interaction parameters, $J_p^{\mathrm{Fe}^\uparrow\mathrm{Fe}^\uparrow}$ (f) and $J_p^{\mathrm{Fe}^\uparrow\mathrm{Fe}^\downarrow}$ (af) in bcc Fe as a function of magnetization, m.

Since the transverse magnetic fluctuations are much faster than the rate of atomic jumps associated with equilibration of atomic configuration, one can define "spin-averaged" effective pair interactions as[80]

$$\begin{aligned} V_p^{(2)} &= \left\langle V_p^{\mathrm{FeCu}} \right\rangle \\ &= \frac{1+m}{2} V_p^{\mathrm{Fe}^\uparrow\mathrm{Cu}} + \frac{1-m}{2} V_p^{\mathrm{Fe}^\downarrow\mathrm{Cu}} + \frac{(1-m^2)}{2} J_p^{\mathrm{Fe}^\uparrow\mathrm{Fe}^\downarrow}, \end{aligned} \tag{10}$$

where $V_p^{\mathrm{Fe}^\uparrow\mathrm{Cu}}$ and $V_p^{\mathrm{Fe}^\downarrow\mathrm{Cu}}$ are the effective pair interactions of Cu with Fe in spin-majority and spin-minority magnetic configurations, respectively. They are different for a nonzero magnetization and become the same in the DLM state. In the ordered FM state, the EI are given by the first term only.

The total effective pair interactions, including the strain-induced contribution, in $Fe_{0.99}Cu_{0.01}$ alloy are shown on Fig. 4 for four different magnetizations. Magnetization strongly affects the interactions at the first coordination shell, by lowering its value by about 10 mRy in the FM state compared with that in the DLM one. Let us note that the contribution of the exchange interactions, $J_1^{\mathrm{Fe}^\uparrow\mathrm{Fe}^\downarrow}$ is only about half of the total effect (see Fig. 3). The other half is due to renormalization of the $V_1^{\mathrm{Fe}^\uparrow\mathrm{Cu}}$ with the magnetization. In other words, the global magnetic state directly affects the chemical interactions in the system. The calculated dependence of the effective pair interactions in Fe-rich Fe-Cu alloys on the state of magnetic order is similar to the one reported previously for Fe-Cr alloys.[80,81]

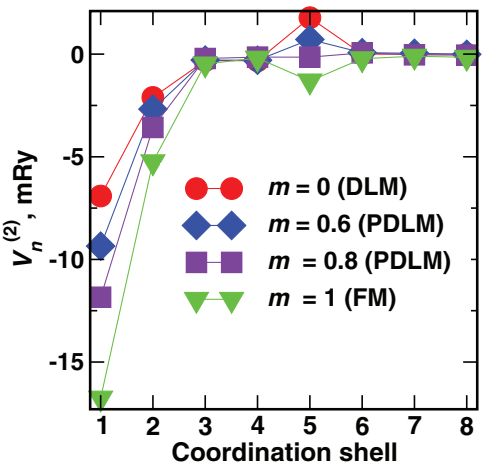

FIG. 4. (Color online) Total effective pair interactions in bcc $Fe_{0.99}Cu_{0.01}$ for different values of magnetization. Negative pair interaction energy corresponds to preferential clustering of two Cu impurities.

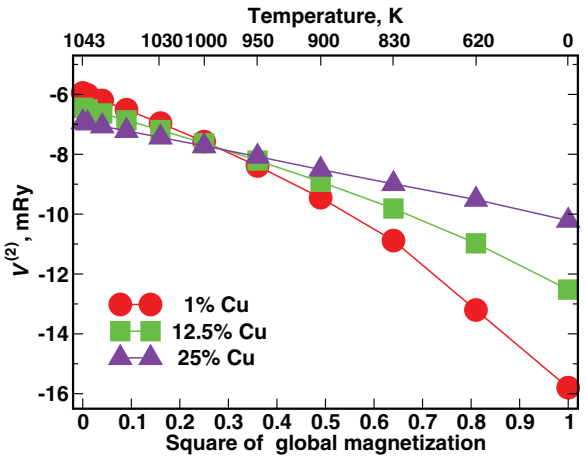

FIG. 5. (Color online) Dependence of the nearest-neighbor effective chemical pair interaction on the square of magnetization for different different alloy compositions. The temperature scale, which matches the value of the global magnetization of Fe, is shown on the top.

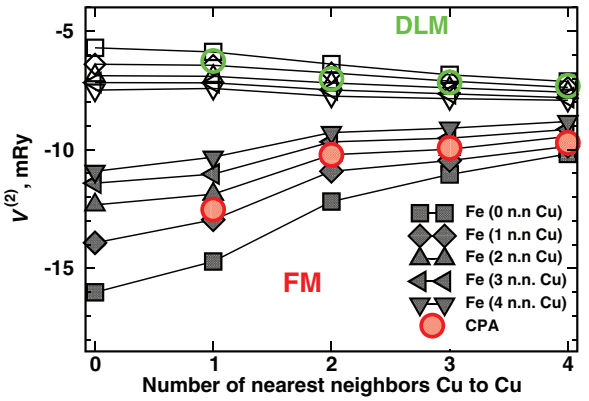

FIG. 6. (Color online) Configuration-dependent effective pair interactions in ferromagnetic (FM, full symbols) and disordered local moment (DLM, open symbols) paramagnetic states, calculated for pairs of Fe and Cu atoms having different numbers of other Cu atoms in the first coordination shell. The corresponding CPA-averaged interactions in random Fe-Cu alloys with 12.5, 25, 33.3, and 50 at.% Cu are shown by circles.

B. Composition and configuration dependencies of the effective interactions

The interactions presented in Fig. 4 have been calculated at a fixed room-temperature experimental volume. While the volume dependence of the EI appears to be weak, the effective interactions are found to be strongly dependent on the alloy composition in the FM state. In Fig. 5, we show the magnetization dependence of the strongest nearest-neighbor chemical interaction for three different alloy compositions: 1, 12.5, and 25 at.% Cu. As a matter of fact, such a concentration dependence can be traced back to changes induced by solute Cu atoms in the *local* electronic and magnetic structure of the alloy, as has been previously elucidated in the case of Fe-Cr alloys.[81]

To demonstrate this, we perform calculations of the effective pair interactions in random Fe-Cu alloys using a *polymorphous* model[105] of a random alloy where every Cu and Fe atom within supercell are different due to their particular local environment. The calculations are done by the LSGF method for 1024-atom supercells with random distributions of Fe and Cu atoms for alloy compositions 6.25, 12.5, 25, and 50 at.% Cu. The local interaction zone of the LSGF method[102,103] has included the nearest-neighbor coordination shell. The calculations have been done at the room-temperature lattice constant in the FM state and at the high-temperature lattice constant in the DLM state.

In Fig. 6, we show the *local-environment* dependent SGPM interactions (i.e., only the chemical contribution), which are statistical *averages* over the four different alloy compositions modeled by the 1024-atom supercells and over all the specific atomic configurations found there that have a given number of Cu nearest neighbors. In other words, these are the effective pair interactions calculated using pairs of Fe and Cu atoms having different numbers of Cu nearest neighbors in the first coordination shell. As one can see, the effective interactions strongly depend on the local environment of the "interacting" atoms in the FM state of the matrix, especially when the number of Cu nearest neighbors varies between 0 and 3.

In Fig. 6, we also show the results of the SGPM-CPA calculations in the framework of an *isomorhpous* model[105] for concentrated Fe alloys with 12.5, 25, 33.3, and 50 at.% Cu, which correspond (on average) to 1, 2, 3, and 4 Cu atoms in the first coordination shell around any atom. It is clear that the CPA results provide a reasonable average magnitude of the local-environment resolved SGPM interactions. However, if one is to describe such a system by the usual Ising model with fixed EI in subsequent statistical simulations, one faces the problem of choosing a single EI value that would be representative of the whole set of concentration- and configuration-dependent EI for every coordination shell.

There is no obvious and definite approach to this problem, although there are very simple arguments in favor of the choice of the EI determined for alloys with higher Cu concentration. The point is that when the temperature is close to the onset of phase separation, Cu atoms start surrounding themselves with other Cu atoms in the nearest-neighbor shell, thereby increasing the local concentration of Cu. Thus the nearest-neighbor interaction makes its thermodynamic contribution when *two* Cu atoms become nearest neighbors, i.e., when each of them has at least one Cu in the nearest-neighbor shell.

In this sense, it is interesting to compare the SGPM calculated results with the results of direct calculations of the nearest-neighbor Cu-Cu interactions in dilute alloys of Cu in Fe, determined as the difference between the total energies of a pair of Cu atoms placed as nearest neighbors and as the most distant neighbors in a given supercell.[140] This interaction has been determined in several previous supercell calculations employing different first-principles methods, yielding quite different results ranging from −10.3 to −18.4 mRy.[63,70,71,129]

Our result for the chemical nearest-neighbor interaction, i.e., without the strain-induced contribution obtained by the PAW method using a 128-atom supercell, is −14.1 mRy. The corresponding LSGF supercell calculations yield −12.4 mRy, the value which is more relevant for comparison with the SGPM results, since it is obtained within the same computational framework. This result is in fact in good agreement with

TABLE I. Calculated total pair interactions $V_n^{(2)-\mathrm{tot}}$ (including both chemical and strain-induced contributions) in the Fe - 12.5 at.% Cu alloy for different values of magnetization. Negative interaction means attraction between Cu atoms. The interactions are in mRy.

n	FM	$m = 0.8$	$m = 0.6$	$m = 0.4$	DLM
1	−13.5	−10.8	−9.2	−8.2	−7.4
2	−3.6	−3.1	−2.6	−2.4	−2.3
3	−0.0	−0.22	−0.3	−0.3	−0.3
4	0.3	−0.1	−0.2	−0.3	−0.3
5	0.1	0.6	1.0	1.4	1.7
6	−0.1	0	0	0	0
7	−0.2	0	0	0	0

the SGPM-LSGF interactions for the case of Fe and Cu having one Cu nearest-neighbor, or the SGPM-CPA interactions for the $Fe_{0.875}Cu_{0.125}$ random alloy. This means that a reasonable choice for statistical thermodynamics simulations of alloy decomposition is a set of EI determined at a high concentration of Cu. In this sense, the Cu clustering at the onset of the phase separation is probably best described by the EI corresponding to concentration of 12.5 at.% Cu, which are presented in Table I.

C. Multisite interactions

Using the SGPM method we have calculated the three-site, $V^{(3)}$, and four-site, $V^{(4)}$ EI in bcc $Fe_{0.875}Cu_{0.125}$ alloy. The strongest three-site interaction is for an atomic chain of the nearest neighbors along the close-packed [111] direction, −2.4 mRy in the FM state and 0.5 mRy in the DLM state. The strongest four-site interaction is for the rhombus of the nearest neighbors in the (110) plane, −4.1 mRy in the FM state and −0.2 mRy in the DLM state. Although these interactions are quite large in the FM state, they become significantly reduced in the PDLM and DLM states. Therefore they have been mostly neglected in our Monte Carlo simulations.

V. SIMULATIONS OF DECOMPOSITION OF Fe-Cu ALLOY

A. Monte Carlo simulations of precipitation temperature

To determine the precipitation start temperature in Fe-Cu alloys, we have performed canonical ensemble[125] MC simulations for Cu alloys within concentration range from 1 to 10 at.% using temperature-dependent (through magnetization) EI. A large simulation box containing about 10^6 atoms has been used in order to minimize the interface energy effects on the solubility limit calculations. Indeed, if N is the number of atoms in a precipitate, then the fraction of Cu atoms at the precipitate-matrix interface may be estimated as $\sim 1/\sqrt{N}$. For the chosen size of the simulation box, and in the case of an alloy with 1% Cu, one expects that about 1 out of 100 Cu atoms will be situated at the interface, which is acceptable for calculating the precipitation.

As has been mentioned above, multisite interactions are relatively small. In particular, we found that the inclusion of the multisite interactions results only in a slight shift of about 10 K of the phase separation temperature. Therefore, to speed up the MC simulations, we have used only effective pair

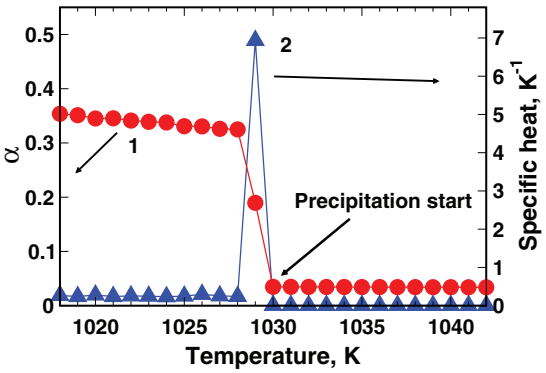

FIG. 7. (Color online) Warren-Cowley SRO parameter α for the first coordination shell (curve 1) and configurational contribution to the heat capacity C_V (curve 2) obtained in the MC simulations for Fe - 1 at.% Cu alloy with the EI for Fe - 12.5 at.% Cu alloy.

interactions up to the seventh coordination shell. The choice of the magnetization for particular temperature has been done using an analytic expression,[141] which relates the temperature to magnetization in bcc Fe.

The temperature of the phase transition (Cu precipitation) has been located using the Warren-Cowley short-range order (SRO) parameter[142] α in the first coordination shell and the specific heat C_V, obtained using the statistical data collected during MC simulations with varying temperature (cooling). In Fig. 7, we show the results of the MC simulations for the alloy containing 1 at.% of Cu. The shapes of $\alpha(T)$ and $C_V(T)$ curves are typical for the first-order phase transition. The width of the apparent transition region decreases with copper concentration. The temperature just above the drastic increase in $\alpha(T)$ was associated with the critical temperature of Cu precipitation $T_0(c)$ for the given concentration c; the error of this procedure was estimated to be about 10 K.

The effective cluster interactions depend on concentration in Fe-Cu alloy (see Sec. IV). Such a dependence may be important at the earliest stage of Cu precipitation when the local concentration increases with time. However, the existing approaches to modeling the decomposition usually neglect this effect. To estimate its magnitude, we have used in our calculations two sets of effective interactions corresponding to compositions Fe - 12.5 at.% Cu (Table I) and Fe - 1 at.% Cu (Fig 4). For temperatures $T < T_C$, we used the EI values calculated at magnetization $m = m(T)$ whose temperature dependence described in Ref. 141; for $T > T_C$, the values of EI corresponding to $m = 0$ have been used.

The so-obtained precipitation temperatures are plotted by open symbols in Fig. 8 in the Arrhenius coordinates $\ln(c)$ versus the inverse temperature $1/T$ for two sets of EI, corresponding to 1 at.% (Fig. 4) and 12.5 at.% (Table I) of Cu in Fe. Available experimental data are shown by filled symbols. As can be seen from Fig. 8, both sets of theoretical results are qualitative agreement with experiment. However, the simulations with the EI corresponding to 12.5 at.% of Cu in Fe are in better agreement with experiment, and predict a higher solubility for $T < T_c$ and lower for $T > T_c$, than the results obtained the set of EI corresponding to Fe - 1 at.% Cu. It means, in our opinion, that Fe - 12.5 at.% Cu composition (when each Cu atom have at least one Cu atom

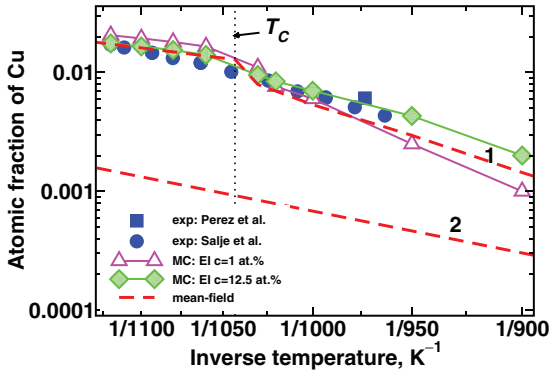

FIG. 8. (Color online) Calculated Cu solubility (onset of clustering) shown together with experimental data (filled circles from Ref. 76 and filled squares from Ref. 35). The Monte Carlo results are shown by open triangles (with the EI calculated for Fe - 1 at.% Cu) and half-filled diamonds (EI for Fe - 12.5 at.% Cu). The dashed lines show the single-site mean-field solubility calculated using magnetization-dependent solution energy (curve 1) or constant solution energy corresponding to the fully ordered FM state (curve 2). The Curie temperature is shown by vertical dotted line.

in first coordination shell) describes better Cu distribution corresponding to the embryo of the precipitate.

The decrease of the apparent solution energy of Cu in bcc Fe above the T_c is due to weakening of the effective nearest-neighbor pair interaction in the PM state as compared to that in the FM state (see Fig. 4). Thus, the change of slope of the solubility line on the Arrhenius plot of Fig. 8 with temperature near T_c originates from the dependence of interactions on the global magnetization.

In Fig. 8, we also show the solubility estimated using a single-site mean-field (MF) approximation based on the solution energy:

$$c = \exp(-E_{\mathrm{sol}}/k_B T). \tag{11}$$

Here, we have used our calculated solution energies, 46.2 mRy in the FM state, and 28.8 mRy in the DLM state (see Sec. III A). For intermediate magnetic states we have used the approximation that the solution energy varies in proportional to the square of magnetization.

As one can see, if the magnetic-dependent solution energies are used, the MF results in the DLM and FM states are in good agreement with experimental data and MC simulations with the EI from 12.5 at.% Cu alloy. However, if one use FM solution energies ($T = 0$), MF results quite different from the MC results in finite temperatures. The origin of the difference is the fact that EI in the MC simulations are dependent on magnetization. Thus it is clear that a substantial increase of the Cu solubility in Fe in the FM state at temperatures close to the Curie temperature has magnetic origin: the interaction between Cu becomes much less repulsive when FM state is weakening.

The results of MC modeling slightly deviate from the experiment[76] above the Curie temperature (see Fig. 8). This discrepancy indicates that the global magnetization is not the only parameter that controls the thermodynamics of bcc Fe based alloys near the magnetic transition. We describe the paramagnetic state within the DLM approximation assuming a completely random distribution of magnetic moments, in the sense that all correlations are absent. At the same time, the magnetic short-range order (MSRO) that is quite pronounced to be strong in bcc Fe well above the T_C[96,143] should contribute to the effective interactions in the paramagnetic state of Fe-Cu. The MSRO may be expected to produce a smoother temperature dependence of the solubility near T_C, while having a slight effect on the value of solubility at higher temperatures. Thus a smooth decrease of magnetization with temperature approaching T_C from below, as well as the presence of MSRO above the T_C, mask the total effect of magnetism on the Cu solubility in bcc Fe, in spite of the substantial difference in the magnitude of effective interactions between the ordered ferromagnetic and disordered paramagnetic states.

B. Kinetics of decomposition

To investigate the kinetics of decomposition in Fe-Cu alloys we have carried out MC simulations using Kawasaki dynamics approach with the *ab initio* effective pair interaction in the first three coordination shell determined in the Fe - 12.5 at.% Cu alloy (see Table I), which allow us well to describe Cu solubility. Our calculations show that the more distant effective pair interactions do not affect qualitatively the transformation kinetics. The set of interactions is chosen according to the magnetization value that corresponds to the temperature of modeling (using an analytic expression suggested in Ref. 141).

Isothermal decomposition of Fe-Cu alloys has been modeled starting from a random distribution of Cu atoms on the lattice sites of a $80 \times 80 \times 80$ supercell built upon a two-atom bcc unit cell subject to periodic boundary conditions. The simulation results are presented in Fig. 9 as a time-temperature-transformation (TTT) diagram, which is usually employed to describe kinetics of isothermal phase transformations.

The TTT diagram shows the time needed to reach a given fraction of decomposition at a fixed temperature. The degree

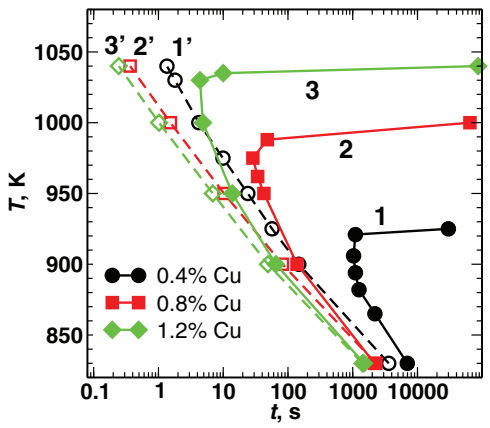

FIG. 9. (Color online) Time-temperature-transformation (TTT) diagram of decomposition of dilute Fe-Cu alloys. It shows the time needed to attain the precipitate volume fraction of 0.2 a given temperature. The curves (1.1'), (2.2'), (3.3') correspond to the alloy concentrations of 0.4, 0.8, and 1.2 at.% Cu. The solid lines (1,2,3) correspond to KMC modeling with PDLM interactions, the dashed lines (1',2',3') correspond to the modeling with FM interactions.

of decomposition was determined as

$$S = \frac{1}{N}\sum_{j=1}^{N}\sigma_j\,\theta\left(\frac{1}{Z}\sum_{k=1}^{Z}\sigma_k^{(j)} - 1\right), \qquad (12)$$

where N is the number of Cu atoms, $\sigma_k^{(j)}$ are the occupation numbers for the nearest-neighbor positions of site j, Z is the number of the nearest neighbors (equal to 8 for bcc lattice), $\theta(x)$ is the Heaviside function. This definition means that a Cu atom is counted as belonging to a precipitate if all its nearest neighbors are also Cu atoms. In other words, we assume (in accordance with the MC thermodynamic simulations) that precipitates contain only Cu atoms and neglect the contributions due to the precipitate-matrix interface when calculating the volume fraction of precipitates.

The c-shaped TTT curve emanates from the combined effect of increasing the driving force for the phase transformation (decomposition) with decreasing the temperature, and decreasing the nucleation and growth rates of precipitates due to the decreasing diffusion rate. Our calculations show that copper clustering does not occur in the PM state at $T > 1043$ K for alloy compositions in the range from 0.4 to 1.2 at.% Cu. In contrast, in the FM state at temperatures below 920 K, the decomposition is already observed for alloys containing as little as 0.4 at.% Cu.

The results of the kinetic MC simulations show that if the EI corresponding to the fully ordered FM state are used at all temperatures (dashed lines in Fig. 9), the position of the nose on TTT curves is not observed in the considered temperature interval, in disagreement with experimental observations.[35] Thus account of the EI variation with temperature approaching to T_C appears necessary for reasonable description of precipitation kinetics in Fe-Cu alloys.

As can be seen from Fig. 9, increasing the Cu concentration accelerates the process of decomposition in Fe-Cu alloys: the nose of TTT curves shifts from 10^3 s at 900 K to 10 s at 1000 K when the Cu concentration is increased from 0.4 to 1.2 at.%. The temperature at which the calculated transformation rate reaches its maximum is in reasonable agreement with that observed in the experiment.[35] In particular, our calculations predict the maximum transformation rate for alloy Fe - 1.2 at.% Cu to correspond to temperature ~1000 K, whereas experimentally the maximum transformation rate was was found at ~950 K for alloy Fe - 1.4 at.% Cu.[35] In the range of temperatures corresponding to the noses on the calculated TTT curves, the corresponding transformation times are in the same order of magnitude as the times observed experimentally. At the same time, our calculations predict much slower precipitation kinetics at lower temperatures than the kinetics obtained in previous theoretical studies such as Ref. 64.

VI. CONCLUSIONS

We have investigated the decomposition in Fe-Cu alloys using first-principles calculations of the effective interactions and subsequent statistical-mechanical (Monte Carlo) simulations of Cu precipitation. We have found that the EI in Fe-Cu alloys are strongly dependent on the global magnetic state of the alloy. This is also reflected in a strong dependence of the Cu impurity solution energy in Fe on the magnetic state. The solution energy is significantly reduced in the PM state compared to that in the FM state.

At the same time, our vibrational free energy calculations show that lattice vibrations most probably play a minor role in the solubility of Cu in Fe at high temperatures. However, further investigation is needed to fully account for the effect of magnetic disorder in the lattice dynamics at temperatures of the order of T_C.

Another important effect, which should be accounted for in the future more accurate theoretical consideration of this system, is the dependence of the effective interactions on the local composition. Although this dependence is much less pronounced in the PM state, it has been shown to be quite substantial in the FM state. In particular, the accounting of the concentration dependence of EI can affect the precipitation kinetics and the precipitate composition. This task requires going beyond the traditional Ising-like model of configuration energetics of alloys. Combined with the still missing accurate account of the vibrational contribution it will be a highly nontrivial task.

ACKNOWLEDGMENTS

A.V.R. is grateful to the Swedish Research Council (VR project 15339-91505-33) and the European Research Council grant. Part of this work was performed within the VINN Excellence Center Hero-m, financed by VINNOVA, the Swedish Government Agency of Innovation Systems, Swedish Industry and the Royal Institute of Technology. P.A.K. acknowledges financial support from the Swedish Research Council (VR project GENIUS) and from SKB, the Swedish Nuclear Fuel and Waste Management Company. The computations were partly performed on resources provided by the Swedish National Infrastructure for Computing (SNIC) at the National Supercomputer Center (NSC) in Linköping, Sweden.

[1] W. C. Leslie and E. Hornbogen, in *Physical Metallurgy*, edited by R. W. Cahn and P. Haasen (North-Holland, Amsterdam, 1996).

[2] K. C. Russell and L. M. Brown, Acta Metall. **20**, 969 (1972).

[3] D. J. Bacon and Yu. N. Osetsky, J. Nucl. Mater. **329–333**, 1233 (2004).

[4] G. R. Odette and G. E. Lucas, Radiat. Eff. Defects Solids **144**, 189 (1998).

[5] S. Vaynman, I. Uslander, and M. E. Fine, *Proceedings of 39th Mechanical Working and Steel Processing Conference, ISS, Indianapolis, Indiana (1997)*, p. 1183; S. Vaynman, R. S. Guico, M. E. Fine, and S. J. Manganello, Metall. Trans. A **28**, 1274 (1997).

[6] S. K. Lahiri, D. Chandra, L. H. Schwartz, and M. E. Fine, Trans. AIME **245**, 1865 (1969).

[7] T. Harry and D. J. Bacon, Acta Mater. **50**, 195 (2002); **50**, 209 (2002).

[8] M. E. Fine, J. Z. Liu, and M. D. Asta, Mater. Sci. Eng. A **463**, 271 (2007).

[9]S. R. Goodman, S. S. Brenner, and J. R. Low, Metall. Trans. **4**, 2363 (1973); **4**, 2371 (1973).
[10]P. J. Othen, M. L. Jenkins, and G. D. W. Smith, Philos. Mag. A **70**, 1 (1994).
[11]M. H. Mathon, A. Barbu, F. Dunstetter, F. Maury, N. Lorenzelli, and C. H. de Novion, J. Nucl. Mater. **245**, 224 (1997).
[12]M. K. Miller, K. F. Russell, P. Pareige, M. J. Starink, and R. C. Thomson, Mater. Sci. Eng. A **250**, 49 (1998).
[13]S. Panwar, D. B. Goel, O. P. Pandey, and K. Satya Prasad, Bull. Mater. Sci. **26**, 441 (2003); **29**, 281 (2006).
[14]A. Cerezo, S. Hirosawa, I. Rozdilsky, and G. D. W. Smith, Philos. Trans. R. Soc. London A **361**, 463 (2003).
[15]D. Isheim, M. S. Gagliano, M. E. Fine, and D. N. Seidman, Acta Mater. **54**, 841 (2006).
[16]S. Vaynman, D. Isheim, R. P. Kolli, S. P. Bhat, D. N. Seidman, and M. E. Fine, Metall. Mater. Trans. A **39A**, 363 (2008).
[17]A. Morley, G. Sha, S. Hiroshava, A. Cerezo, and G. D. W. Smith, Ultramicroscopy **109**, 535 (2009).
[18]S. M. He, N. H. van Dijk, H. Schut, E. R. Peekstok, and S. van der Zwaag, Phys. Rev. B **81**, 094103 (2010).
[19]R. Shabadi, R. Taillard, B. Radiguet, J. de Baerdemaeker, and E. Leunis, Solid State Phenomena **172–174**, 297 (2011).
[20]R. P. Kolli, Z. Mao, and D. N. Seidman, Appl. Phys. Lett. **91**, 241903 (2007).
[21]R. P. Kolli and D. N. Seidman, Microsc. Microanal. **13**, 272 (2007).
[22]A. S. Murthy, J. E. Medvedeva, D. Isheim, S. L. Lekakh, V. L. Richards, and D. C. Van Aken, Scripta Mater. **66**, 943 (2012).
[23]G. M. Worrall, J. T. Buswell, C. A. English, M. G. Hetherington, and G. D. W. Smith, J. Nucl. Mater. **148**, 107 (1987).
[24]F. Maury, A. Lucasson, P. Lucasson, P. Maser, and F. Faudot, J. Phys.: Condens. Matter **2**, 9291 (1990).
[25]F. Maury, N. Lorenzelli, C.-H. de Novion, and P. Lagarde, Scripta Metall. Mater. **25**, 1839 (1991).
[26]F. Maury, N. Lorenzelli, and C. H. De Novion, J. Nucl. Mater. **183**, 217 (1991).
[27]T. N. Le, A. Barbu, D. Liu, and F. Maury, Scripta Metall. **26**, 771 (1992).
[28]F. Maury, N. Lorenzelli, M. H. Mathon, C. H. de Novion, and P. Lagarde, J. Phys.: Condens. Matter **6**, 569 (1994).
[29]P. Auger, P. Pareige, M. Akamatsu, and D. Blavette, J. Nucl. Mater. **225**, 225 (1995).
[30]H. A. Hardouin Duparc, R. C. Dole, M. L. Jenkins, and A. Barbu, Philos. Mag. Lett. **71**, 325 (1995).
[31]P. Auger, P. Pareige, S. Welzel, J-C. Van Duysen, J. Nucl. Mater. **280**, 331 (2000).
[32]A. Barbu, T. N. Le, N. Lorenzelli, F. Maury, and C.-H. de Novion, Annales De Chimie-Science Des Materiaux **16**, 325 (1991).
[33]P. Pareige, F. Perocheau, P. Auger, A. Jumel, and H. Bernas, Nucl. Instrum. Methods Phys. Res., Sect. B **178**, 233 (2001).
[34]Y. Nagai, Z. Tang, M. Hassegawa, T. Kanai, and M. Saneyasu, Phys. Rev. B **63**, 134110 (2001).
[35]M. Perez, F. Perrard, V. Massardier, X. Kleber, A. Deschamps, H. de Monestrol, P. Pareige, and G. Covarel, Philos. Mag. **85**, 2197 (2005).
[36]Y. Nagai, T. Toyama, Y. Nishiyama, M. Suzuki, Z. Tang, and M. Hasegawa, Appl. Phys. Lett. **87**, 261920 (2005).
[37]S. C. Glade, B. D. Wirth, G. R. Odette, P. Asoka-Kumar, P. A. Sterne, and R. H. Howell, Philos. Mag. **85**, 629 (2005).
[38]S. C. Glade, B. D. Wirth, G. R. Odette, and P. Asoka-Kumar, J. Nucl. Mater. **351**, 197 (2006).
[39]Q. Xu, T. Yoshiie, and K. Sato, Phys. Rev. B **73**, 134115 (2006).
[40]J. Saroun, J. Kocik, E. Garcia-Matres, O. Muransky, and P. Strunz, Z. Kristallogr. Suppl. **23**, 393 (2006).
[41]Qiu Xu, Toshimasa Yoshiie, and Koichi Sato, Phys. Status Solidi C **4**, 3573 (2007).
[42]B. Radiguet, A. Barbu, and P. Pareige, J. Nucl. Mater. **360**, 104 (2007).
[43]Q. Xu and T. Yoshiie, Phil. Mag. **91**, 3716 (2011).
[44]H. R. Habibi, Mater. Lett. **59**, 1824 (2005).
[45]J. J. Blackstock and G. J. Ackland, Philos. Mag. A **81**, 2127 (2001).
[46]A. Deschamps, M. Militzer, and W. J. Poole, ISIJ Int. **41**, 196 (2001).
[47]P. J. Othen, M. L. Jenkins, G. D. W. Smith, and W. J. Pythian, Philos. Mag. Lett. **64**, 383 (1991).
[48]N. I. Medvedeva, A. S. Murthy, V. L. Richards, D. C. Van Aken, and J. E. Medvedeva, J. Mater. Sci. **48**, 1377 (2013).
[49]M. Schober, E. Eidenberger, H. Leitner, P. Staron, D. Reith, and R. Podloucky, Appl. Phys. A **99**, 697 (2010).
[50]M. Schober, E. Eidenberger, P. Staron, and H. Leitner, Microsc. Microanal. **17**, 26 (2011).
[51]K. Sumiyama, Y. Yoshitake, and Y. Nakamura, Acta Metall. **33**, 1785 (1985).
[52]T. Koyama and H. Onodera, Mater. Trans. **46**, 1187 (2005).
[53]C. Zhang and M. Enomoto, Acta Mater. **54**, 4183 (2006).
[54]T. Nagano and M. Enomoto, Scripta Mater. **55**, 223 (2006).
[55]T. Koyama and H. Onodera, Mater. Sci. Forum **539–543**, 2383 (2007).
[56]R. S. Qin and H. K. Bhadeshia, Mater. Sci. Technol. **26**, 803 (2010).
[57]K. Yu. Khromov, F. Soisson, A. Yu. Stroev and V. G. Vaks, J. Exp. Theor. Phys. **112**, 414 (2011).
[58]V. G. Vaks, F. Soisson, and I. A. Zhuravlev, Philos. Mag. **93**, 3084 (2013).
[59]F. Soisson. A. Barbu, and G. Martin, Acta Mater. **44**, 3789 (1996).
[60]Y. Le Bouar and F. Soisson, Phys. Rev. B **65**, 094103 (2002).
[61]S. Schmauder and P. Binkele, Comput. Mater. Sci. **24**, 42 (2002).
[62]O. Khrushcheva, E. E. Zhurkin, L. Malerba, C. S. Becquart, C. Domain, and M. Hou, Nucl. Instrum. Methods Phys. Res., Sect. B **202**, 68 (2003).
[63]E. Vincent, C. S. Becquart, and C. Domain, J. Nucl. Mater. **351**, 88 (2006).
[64]F. Soisson and C.-C. Fu, Phys. Rev. B **76**, 214102 (2007).
[65]P. R. Monasterio, B. D. Wirth, and G. R. Odette, J. Nucl. Mater. **361**, 127 (2007).
[66]E. Vincent, C. S. Becquart, C. Pareige, P. Pareige, and C. Domain, J. Nucl. Mater. **373**, 387 (2008).
[67]P. Warczok, Y. Shan, M. Schober, H. Leitner, and E. Kozeschnik, Sol. St. Phenom. **172–174**, 309 (2011).
[68]N. Castin, M. I. Pascuet, and L. Malerba, J. Chem. Phys. **135**, 064502 (2011).
[69]J. Z. Liu, A. van de Walle, G. Ghosh, and M. Asta, Phys. Rev. B **72**, 144109 (2005).
[70]C. Domain and C. S. Becquart, Phys. Rev. B **65**, 024103 (2001).
[71]P. Olsson, T. P. C. Klaver, and C. Domain, Phys. Rev. B **81**, 054102 (2010).
[72]D. Reith and R. Podloucky, Phys. Rev. B **80**, 054108 (2009).
[73]D. Reith, M. Stöhr, R. Podloucky, T. C. Kerscher, and S. Müller, Phys. Rev. B **86**, 020201 (2012).
[74]M. Talati, M. Posselt, G. Bonny, A. Al-Motasem, and F. Bergner, J. Phys.: Condens. Matter **24**, 225402 (2012).

[75]H. Harvig, G. Kirchner, and M. Hillert, Metall. Trans. **3**, 329 (1972).
[76]G. Salje and M. Feller-Knipmeier, J. Appl. Phys. **48**, 1833 (1977).
[77]L. H. Chen, T. S. Chin, and M. Hung, J. Appl. Phys. **64**, 5962 (1988).
[78]T. Nishizawa, M. Hasebe, and M. Ko, Acta Metallurgica **27**, 817 (1979).
[79]V. Pierron-Bohnes, M. C. Cadeville, A. Finel, and O. Schaerpf, J. Phys. I France **1**, 247 (1991).
[80]A. V. Ruban, P. A. Korzhavyi, and B. Johansson, Phys. Rev. B **77**, 094436 (2008).
[81]P. A. Korzhavyi, A. V. Ruban, J. Odqvist, J. O. Nilsson, and B. Johansson. Phys. Rev. B **79**, 054202 (2009).
[82]O. I. Gorbatov, P. A. Korzhavyi, A. V. Ruban, B. Johansson, and Yu. N. Gornostyrev, J. Nucl. Mater. **419**, 248 (2011).
[83]M. Rahaman, A. V. Ruban, A. Mookerjee, and B. Johansson, Phys. Rev. B **83**, 054202 (2011).
[84]O. I. Gorbatov, A. V. Ruban, P. A. Korzhavyi, and Yu. N. Gornostyrev, Mater. Res. Soc. Symp. Proc. **1193**, 469 (2009).
[85]O. I. Gorbatov, P. A. Korzhavyi, Yu. N. Gornostyrev, and A. V. Ruban, Sol. St. Phenom. **172–174**, 979 (2011).
[86]C. Zener, Trans. AIME **167**, 550 (1946).
[87]C. Zener, Trans. AIME **203**, 619 (1955).
[88]L. Kaufman, E. V. Clougherty, and R. J. Weiss, Acta Metallurgica **11**, 323 (1963)
[89]M. Hillert, T. Wada, and H. Wada, J. Iron Steel Inst. **205**, 539 (1967).
[90]M. Hillert and M. Jarl, Calphad **2**, 227 (1978).
[91]G. Inden, Physica B & C **103**, 82 (1981).
[92]M. Hillert, J. Appl. Phys. **60**, 1868 (1986).
[93]B. Jönsson, Z. Metallkd. **83**, 349 (1992).
[94]Y. Liu, L. Zhang, Y. Du, and D. Liang, CALPHAD: Comput. Coupling Phase Diagrams Thermochem. **33**, 732 (2009).
[95]W. Xiong, Q. Chen, P. A. Korzhavyi, and M. Selleby, CALPHAD: Comput. Coupling Phase Diagrams Thermochem. **39**, 11 (2012).
[96]A. V. Ruban and V. I. Razumovskiy, Phys. Rev. B **86**, 174111 (2012).
[97]L. Vitos, H. L. Skriver, B. Johansson, and J. Kollar, Comput. Mater. Sci. **18**, 24 (2000).
[98]L. Vitos, Phys. Rev. B **64**, 014107 (2001).
[99]L. Vitos, I. A. Abrikosov, and B. Johansson, Phys. Rev. Lett. **87**, 156401 (2001).
[100]L. Vitos, *Computational Quantum Mechanics for Materials Engineers* (Springer-Verlag, London, 2007).
[101]P. Soven, Phys. Rev. **156**, 809 (1967); B. L. Györffy, Phys. Rev. B **5**, 2382 (1972).
[102]I. A. Abrikosov, A. M. N. Niklasson, S. I. Simak, B. Johansson, A. V. Ruban, and H. L. Skriver, Phys. Rev. Lett. **76**, 4203 (1996).
[103]I. A. Abrikosov, S. I. Simak, B. Johansson, A. V. Ruban, and H. L. Skriver, Phys. Rev. B **56**, 9319 (1997).
[104]O. E. Peil, A. V. Ruban, and B. Johansson, Phys. Rev. B **85**, 165140 (2012).
[105]A. V. Ruban and H. L. Skriver, Phys. Rev. B **66**, 024201 (2002); A. V. Ruban, S. I. Simak, P. A. Korzhavyi, and H. L. Skriver, *ibid.* **66**, 024202 (2002).
[106]B. L. Gyorffy, A. J. Pindor, G. M. Stocks, and H. Winter, J. Magn. Magn. Mater. **45**, 15 (1984).
[107]B. L. Gyorffy, A. J. Pindor, J. B. Staunton, G. M. Stocks, and H. Winter, J. Phys. F: Met. Phys. **15**, 1337 (1985).
[108]J. P. Perdew, K. Burke, and M. Ernzerhof, Phys. Rev. Lett. **77**, 3865 (1996).
[109]H. J. Monkhorst and J. D. Pack, Phys. Rev. B **13**, 5188 (1976).
[110]A. V. Ruban, S. Shallcross, S. I. Simak, and H. L. Skriver, Phys. Rev. B **70**, 125115 (2004).
[111]Z. S. Basinski, W. Hume-Rothery, and A. L. Sutton, Proc. R. Soc. London A **229**, 459 (1955).
[112]I. Seki and K. Nagata, ISIJ Int. **45**, 1789 (2005).
[113]S. G. E. Te Velthuis, J. H. Root, J. Sietsma, M. Th. Rekveldt, and S. van der Zwaag, Acta Mater. **46**, 5223 (1998).
[114]Calculations at the theoretical lattice parameters (obtained using the classical Debye-Grüneisen model) yield quantitatively very similar results, so the picture of the influence of magnetism on the precipitation remains the same.
[115]P. E. Blöchl, Phys. Rev. B **50**, 17953 (1994).
[116]G. Kresse and D. Joubert, Phys. Rev. B **59**, 1758 (1999).
[117]G. Kresse and J. Hafner, Phys. Rev. B **47**, 558 (1993).
[118]G. Kresse and J. Hafner, Phys. Rev. B **49**, 14251 (1994).
[119]G. Kresse and J. Furthmuller, Phys. Rev. B **54**, 11169 (1996).
[120]G. Kresse, J. Furthmuller, and J. Hafner, Europhys. Lett. **32**, 729 (1995).
[121]O. E. Peil, A. V. Ruban, and B. Johansson, Phys. Rev. B **79**, 024428 (2009).
[122]B. Schönfeld, M. Engelke, and A. V. Ruban, Phys. Rev. B **79**, 064201 (2009).
[123]O. I. Gorbatov, A. R. Kuznetsov, Yu. N. Gornostyrev, A. V. Ruban, N. V. Ershov, V. A. Lukshina, Yu. P. Chernenkov, and V. I. Fedorov, J. Exp. Theor. Physics **112**, 848 (2011).
[124]O. I. Gorbatov, Yu. N. Gornostyrev, A. R. Kuznetsov, and A. V. Ruban, Sol. St. Phenom. **172–174**, 618 (2011).
[125]K. Binder, *Applications of the Monte Carlo method in Statistical Physics* (Springer, Berlin, 1984).
[126]K. Kawasaki, in *Phase Transitions and Critical Phenomena*, edited by C. Domb and M. S. Green (Academic, New York, 1972), Vol. 2, p. 443.
[127]J. Dai, J. M. Kanter, S. S. Kapur, W. D. Seider, and T. Sinno, Phys. Rev. B **72**, 134102 (2005).
[128]S. I. Golubov, A. Serra, Yu. N. Osetsky, and A. V. Barashev, J. Nucl. Mater. **277**, 113 (2000).
[129]O. I. Gorbatov, S. V. Okatov, Yu. N. Gornostyrev, P. A. Korzhavyi, and A. V. Ruban, Phys. Met. Metallogr. **114**, 642 (2013).
[130]S. Baroni, S. de Gironcoli, A. Dal Corso, and P. Giannozzi, Rev. Mod. Phys. **73**, 515 (2001).
[131]S. Baroni, P. Giannozzi, and A. Testa, Phys. Rev. Lett. **58**, 1861 (1987).
[132]X. Gonze and C. Lee, Phys. Rev. B **55**, 10355 (1997).
[133]http://phonopy.sourceforge.net/.
[134]Atsushi Togo, Fumiyasu Oba, and Isao Tanaka, Phys. Rev. B **78**, 134106 (2008).
[135]V. I. Razumovskiy, A. V. Ruban, and P. A. Korzhavyi, Phys. Rev. Lett. **107**, 205504 (2011).
[136]I. Leonov, A. I. Poteryaev, V. I. Anisimov, and D. Vollhardt, Phys. Rev. B **85**, 020401 (2012).
[137]A. V. Ruban and V. I. Razumovskiy, Phys. Rev. B **85**, 174407 (2012).

[138] A. Liechtenstein, M. I. Katsnelson, and V. A. Gubanov, J. Phys. F: Met. Phys. **14**, L125 (1984); A. Liechtenstein, M. I. Katsnelson, V. P. Antropov, and V. A. Gubanov, J. Magn. Magn. Mater. **67**, 65 (1987).

[139] V. Heine, A. I. Lichtenstein, and O. N. Mryasov, Europhys. Lett. **12**, 545 (1990).

[140] The so-obtained pair interactions are equal to the effective pair interactions only if multisite interactions are vanishingly small [see A. V. Ruban and I. A. Abrikosov, Rep. Prog. Phys. **71**, 046501 (2008)].

[141] M. D. Kuz'min, Phys. Rev. Lett. **94**, 107204 (2005).

[142] J. M. Cowley, Phys. Rev. **77**, 669 (1950); **120**, 1648 (1960).

[143] X. Tao, D. P. Landau, T. C. Schulthess, and G. M. Stocks, Phys. Rev. Lett. **95**, 087207 (2005)